J. Fluid Mech. (1979), *vol.* 94, *part* 1, *pp.* 39–64
Printed in Great Britain

Mean flow generation by topographic Rossby waves

By ALAIN COLIN DE VERDIERE†
Woods Hole Oceanographic Institution, Woods Hole, Massachussetts 02543

(Received 1 May 1978)

This paper makes use of the ease of modelling topographic Rossby waves in a laboratory context to investigate the ability of these waves to generate strong zonal mean flows when the geostrophic (f/H) contours are closed. A zonally travelling wave is forced in a narrow latitude band of a 'polar beta plane'. Stronger signals occur when the motion of the driving is retrograde and at the phase speed of the gravest free modes. An important zonal westward mean flow occurs in the free interior while a compensating eastward jet is found at forced latitudes. The dependence of the mean flow strength upon the wave steepness indicates that genuine rectification processes are indeed taking place when the fluid is stirred by purely oscillating devices.

This general tendency for topographic Rossby waves to transfer energy to zonal components is first analysed theoretically by investigating a side-band instability mechanism within an unforced fluid. Among the products of the interactions between a primary wave of wavenumber $\mathbf{k}$ and its side bands of wavenumber $\mathbf{k} \pm \delta\mathbf{k}$, the zonal flow is prominent. Wave steepnesses of order $(|\delta\mathbf{k}|/|\mathbf{k}|)^{\frac{1}{2}}$ only are required for zonal energy to grow whereas non-zonal components of scale longer or shorter than the primary wave need huge steepnesses [of order $(|\delta\mathbf{k}|/|\mathbf{k}|^{-\frac{3}{2}}$] for amplification. This supplements the earlier notion that 'nearly zonal' waves may be generated by weak resonant interaction.

For gentle driving certain classical aspects of Rossby wave propagation can be checked against the experiments. The linear theory provides also a convenient framework to discuss the meridional structure of the wave-induced Reynolds stress. For more energetic driving, a test of the potential vorticity mixing theory can be carried out and sheds further light upon the rectification mechanisms.

1. Introduction

It is of utmost interest in the atmosphere and in the ocean to be able to distinguish between externally forced mean flows and those driven by the mesoscale turbulence in which they are embedded. The early wind-driven theory of the oceanic general circulation of Stommel (1948) provided a picture of the first class of flows. The discovery of a very energetic oceanic weather obscuring this general circulation has prompted the study of eddy-driven mean flows to understand their role in global ocean dynamics.

The subject has a long atmospheric history: a few decades ago, meteorologists were faced with the problem of explaining the energy and momentum transfer between the surface mid-latitude westerlies and the large-scale perturbations therefrom. The

† Permanent address: Centre Océanologique de Bretagne, B.P. 337, 29273 Brest Cédex, France.

0022-1120/79/4204-6410 $02.00

concept of negative viscosity was then introduced by Starr (1968) to describe the possible transfers from the turbulence to the mean flow.

Rossby wave properties were invoked in an oceanic context by Thompson (1971) to explain the systematically negative Reynolds stresses $\overline{uv}$ of long period motions at a site due north of the Gulf Stream. The latter was suggested as a likely energy source for the relevant dispersion relation associates a northward group velocity with negative stresses. In the meantime the modelling of unsteady planetary flows in the laboratory has already reached an advanced stage with studies by Phillips & Ibbetson (1967) and Beardsley (1969, 1975) among others, these studies having focused on realizations of flows governed by linear theory or small deviations therefrom. Whitehead (1975) was the first to show experimentally that zonal jets could be produced on a beta plane stirred by energetic oscillatory processes.

The plan of this paper is as follows. Experimental techniques are presented in §2. Section 3 is an account of the salient features of the laboratory runs. They demonstrate readily that finite amplitude topographic Rossby waves are capable of producing significant mean currents along geostrophic contours. Intensive measurements of the flow are made to quantify various features of the interaction. Theoretical approaches to the mean flow generation processes are then investigated in §4. The interaction of discrete planetary waves on an unforced infinite beta plane is extended to the situation which prevails when conditions for the existence of weakly resonant triads are not met. The interaction of a finite amplitude primary wave with some residual side-band noise is then seen to force zonal flows by an amplitude selection mechanism on a time scale short compared with the modulation period of the zonal flow. This linear stability analysis is particularly relevant to the transient evolution of free turbulence on a beta plane. For closer connexion with the experiments involving forced flows with dissipation, both the wave radiation approach and the potential vorticity mixing theory are used in complementary ways at various amplitude levels and tested quantitatively in §5. This last part contains also an account of the decay of the waves in the presence of their self-induced mean flows when the wave driving is impulsively turned off.

2. Description of the experiments

The idea of the experiment originated from Dr A. McEwan, who must also be credited with the various designs of the components needed for this study. The wave tank is a plastic cylinder 62 cm in diameter and 30 cm in height. The axis of the cylinder coincides with the axis of the rotating table itself parallel to the local gravity vector within 4 s of arc. The topography needed to simulate the beta effect is introduced by allowing the free surface to adjust as a paraboloid under the rotational constraint. The geostrophic f/H contours are thus circular with the equivalent beta increasing linearly from the centre to the outer wall. Earlier workers modelling planetary flows have used a wide variety of forcing mechanisms. To generate relative vorticity efficiently, the use of a distribution of sources and sinks at the bottom of the tank appears to be most satisfactory. It has also the added advantage of modelling rather well the forcing mechanisms of large-scale geophysical flows. In the present work, a zonally travelling wave of mode number 12 is forced in a narrow annular region close to the outer wall, by a periodic distribution of sources and sinks. A total

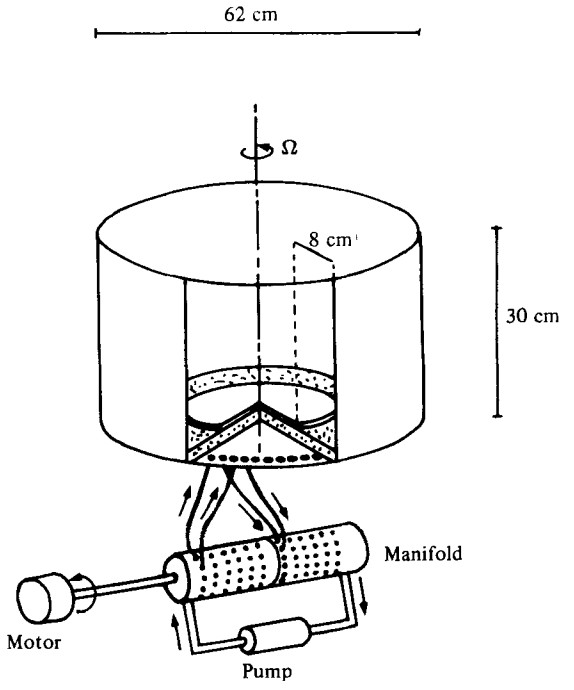

FIGURE 1. Overall view of the experimental set-up.

number of 72 sources and 72 sinks are arranged around the tank as in figure 1. In the present arrangement, the sources and sinks cannot exchange roles as they may only be switched on or off. A wavelength of the forcing pattern therefore consists of six sources and six sinks, only three of each being turned on at any given time. The manifold which is used to make the pattern periodic and zonally propagating is the genuine fluid commutator shown in figure 2(*a*). A sealed plastic pipe is divided into two independent source and sink sections. On the inside it is fitted with a rotating shaft which enables one to open and close the holes drilled at the periphery of the pipe as it rotates. A centrifugal pump is connected between the two sections. Therefore fluid entering the manifold from the pump is expelled through the peripheral holes to the sources at the bottom of the tank by thin plastic tubes of equal length. The return path starts from the bottom sinks, enters the forcing manifold through the sink section and continues outwards to the pump. Figure 1 illustrates this point for a sample source and sink. It remains to understand how the manifold can make the forcing pattern propagate zonally. Figure 2(*b*) explains schematically the phase relationship which exists between bottom sources and sinks and the position of the connecting tubes around the fluid commutator. Two forcing wavelengths are illustrated. It is clear that if, for instance, the shaft rotates clockwise the pattern will propagate anticlockwise, half a turn of the shaft corresponding to a full period of the forcing pattern. The shaft rotation is produced by a high torque, low r.p.m. electric motor. Thus both the amplitude and the phase speed of the forced wave can be adjusted by varying the pump flow rate and the shaft rotation rate respectively. Sources and sinks are covered by a 2 cm thick layer of foam rubber to avoid jetting effects at the mouth of the tubes. Away from this area (8 cm wide), the bottom is covered by a flat metallic plate as can be seen in figure 1.

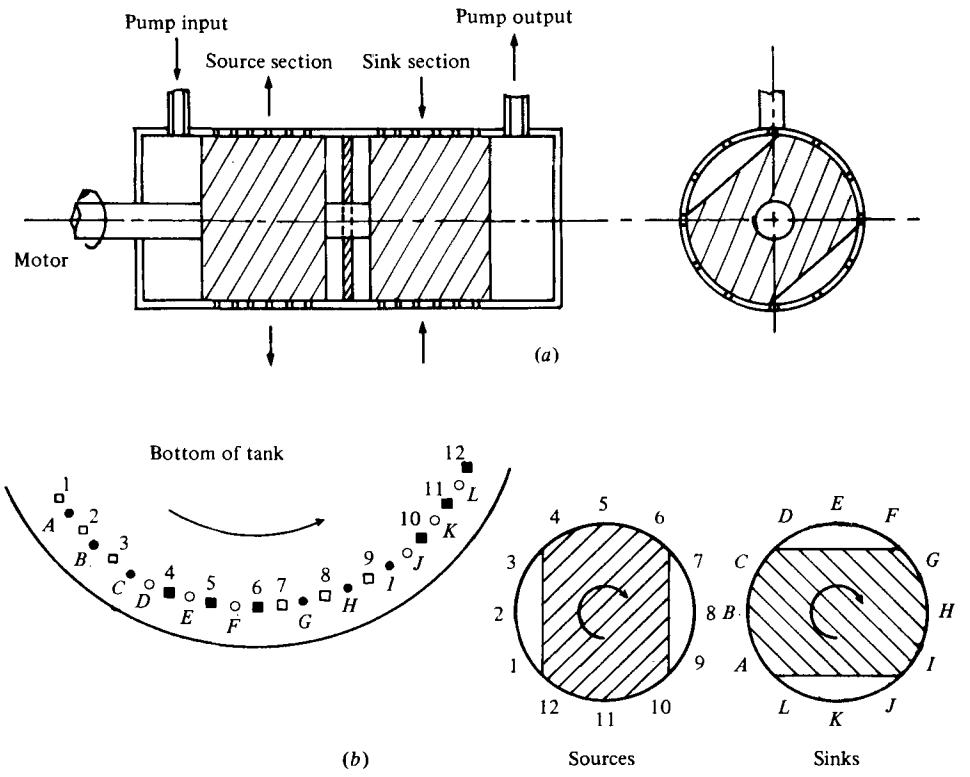

FIGURE 2. (*a*) The forcing manifold: a hydraulic commutator. (*b*) Diagram showing the phase relationship between bottom sources and sinks and corresponding positions on the manifold. ■, source off; □, source on; ●, sink on; ○, sink off.

The measurements were made in two ways: optically, by taking photographs and films of small (0·5 mm), almost neutrally buoyant polystyrene beads distributed on the free surface; electrically, by sensing the small fluctuations of the free-surface elevation with two capacitance probes one situated within the forced region, the other in the free interior. These two methods are complementary since the former provides spatial information while the latter allows a look at the temporal variability.

Choice of the experimental parameters is somewhat restricted if one wants to look at quasigeostrophic motions with Ekman friction kept at a minimum. Quasigeostrophy requires that the fractional depth change be small on the scale of the low frequency motions. This turns out to be a condition of small Froude number

$$Fr = \Omega^2 L^2/gH$$

for our particular topography, which is

$$H = H_0 + \tfrac{1}{2}\Omega^2 r^2,$$

Ω being the rotation rate, L the scale of the motion, g the acceleration due to gravity and H the depth. A conflicting situation is met if one attempts to increase the resonance of the Rossby modes. Since viscous effects are essentially controlled by Ekman dynamics, the non-dimensional number governing the degree of inviscidness of the waves is the ratio of the wave period to the Ekman spin-up time. Since this ratio is depth independent and varies with rotation as $\Omega^{-\frac{1}{2}}$, higher rotation rates must be

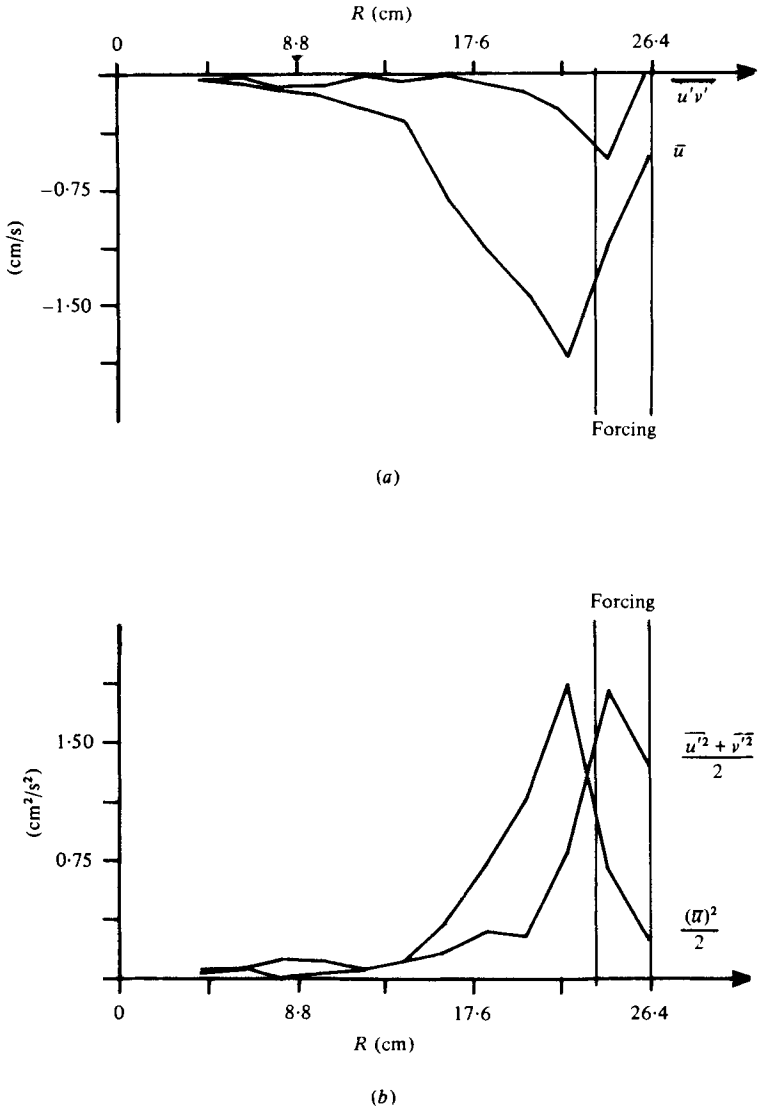

FIGURE 4. The zonally averaged fields as a function of radial distance in the statistically steady state. (*a*) Westward mean flow and Reynolds stress. (*b*) Eddy and mean kinetic energy. In this run the laboratory parameter values are as in figure 6 (plate 2).

used to keep it small. Clearly a compromise must be reached to keep the Froude number small too.

The forcing frequencies are within the frequency range of the gravest Rossby modes. The amplitudes of the motions are such that the Rossby number $U/\Omega L$ is small (10^{-2}) while the wave steepnesses U/c are arbitrary (c being the phase speed of the waves and U a measured r.m.s. particle velocity). The main results will now be presented while more specific measurements will be mentioned at the appropriate sections.

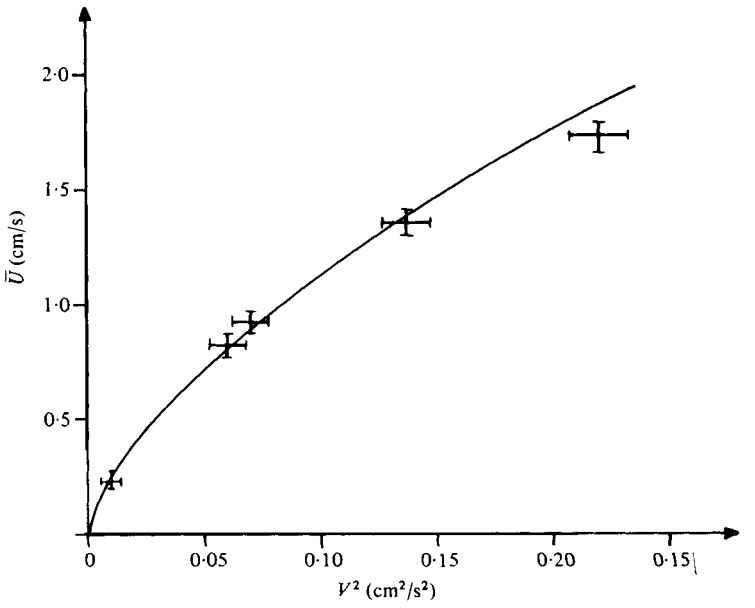

FIGURE 5. The mean flow strength *vs.* the meridional kinetic energy for several runs carried out at various forcing amplitude levels. The solid curve obeys the relationship $\bar{U} = 4{\cdot}93(\overline{V'^2})^{0{\cdot}44}$.

3. Experimental procedures and results

Typical experiments are run as follows: when a state of rest is obtained in the rotating frame, the oscillatory forcing is impulsively turned on. To excite Rossby waves efficiently, the forcing pattern is moved in a retrograde sense. Figure 3(*a*) (plate 1) reveals the transient flows as wave energy moves inwards. The strong southeast–northwest tilt of the eddies should be noticed. Within a few spin-up times, the flow evolves towards a statistically steady state depicted in figure 3(*b*) (plate 1). Since the wave steepness is large in this run, a powerful retrograde mean flow (in either a zonally or a time-averaged sense) develops in the interior while a prograde jet swings along the outer wall in the forced area. The details of the latter are unfortunately hard to detect owing to lighting deficiencies. At any rate the meridional distribution of the jets is reminiscent of the zonal deformation of radial dye lines as observed by Whitehead (1976). Furthermore one can see that the strength of the cyclonic vortices clearly exceeds that of the anticyclonic ones over the forced area.

Velocity measurements have been carried out in this statistically steady state to obtain the north–south profile of Eulerian statistics. Current speeds were measured from streak photographs at 20 equally spaced points around a given latitude circle. Mean velocities and Reynolds-stress tensor were then computed for about ten latitudes, the sampling distance between latitudes being 2·5 cm.

Figure 4(*a*) shows the zonal average of the westward flow and the Reynolds stress as a function of radial distance, while figure 4(*b*) depicts the behaviour of the mean and eddy kinetic energy. The gross meridional distribution of the Reynolds stress is what is needed to balance the viscous losses of the westward mean flow in the interior. The eddy kinetic energy peaks at the forcing and then decays slowly towards the interior. On the other hand the mean kinetic energy peaks somewhat away from the

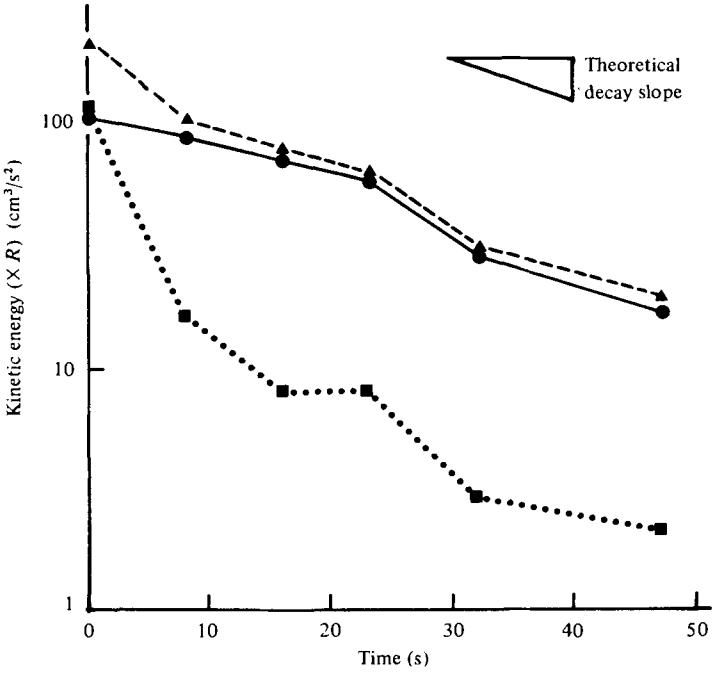

FIGURE 7. Temporal decay of mean and eddy kinetic energy. The quantities plotted are spatial averages of the kinetic energies over the basin. ▲, total kinetic energy; ●, mean kinetic energy; ■, eddy kinetic energy.

forcing. This already indicates the main ingredients needed to maintain a retrograde flow, namely some eddy kinetic energy away from a directly forced region.

In several runs the amplitude of the forcing was varied, everything else being kept the same. The mean circulation and the meridional eddy kinetic energy were measured at a given latitude $R = 23$ cm. The results are plotted on figure 5. As expected, the mean $\bar{U}$ is a growing function of $\overline{v'^2}$ for these runs but the interesting point is that $\bar{U}$ scales on a velocity somewhere between $\overline{v'^2}$ and $(\overline{v'^2})^{\frac{1}{2}}$, the best fit being indicated by the curve which satisfies the following power law:

$$\bar{U} = 4{\cdot}93(\overline{v'^2})^{0{\cdot}64}.$$

This has important consequences which will be considered in detail in §5, but this reinforces our conviction that we are witnessing the generation of genuine eddy-driven mean flows.

This general presentation would not be complete without mention of the period of decay from the statistically steady state. Figure 6 (plate 2) depicts the evolution towards a state of rest. One cannot help being struck by the unequal disappearance of mean and fluctuating kinetic energy. The use of the pressure probes also revealed a wave damping occurring at a rate much smaller than the Ekman time scale. To test the idea further, spatial averaging of both mean and fluctuating kinetic energy was achieved as a function of decay time. Velocities were measured at ten equally spaced points around concentric latitude circles and this was done for 11 latitudes. This represents a data base of 110 values which spatial statistics can be constructed upon.

The results shown on figure 7 reveal the slow (fast) decay of the mean (eddy) kinetic energy on the Ekman time scale. On the other hand the total kinetic energy decays with the appropriate viscous time scales.

These experiments as well as others suggest that barotropic Rossby waves tend to release their energy preferentially to zonal Fourier components. The next section presents a theory dealing with the instability of a primary wave in the presence of seed energy in adjacent side bands.

4. Generation of zonal flows by Rossby wave side-band instabilities

The subject of zonal flow generation by interacting Rossby waves has a long history in view of its potential significance for atmospheric motions of planetary scale.

Longuet-Higgins & Gill (1967) applied the newly developed weak resonant interaction theory and showed that discrete waves were unable to feed energy into a mean zonal flow. Later Newell (1969) and more recently Loesch (1977) used Rossby wave packets rather than infinite plane waves and found that on an infinite beta plane the resonant theory could lead to a transfer of energy to a zonal flow but in a characteristic time much longer than that of the triad interaction, revealing the weaknesses of the mechanism. Both Loesch (1977) and Plumb (1977) found that, in a zonal channel geometry, Rossby waves are unstable to second-order resonant interactions, the end result being that zonal waves are generated faster on the time scale of the triad interaction itself. However these results do not cover the turbulent stages of the present controlled laboratory experiments and others with higher levels of nonlinearity. In a numerical context, Rhines's (1975) calculations may be recalled. Filling initially his periodic ocean with small-scale nonlinear eddies, he let the flow evolve freely according to the beta-plane equations. The familiar energy cascade to the large-scale motions occurs but slows down when the wave steepness becomes of order unity. At the same time the flow has become highly anisotropic with eddies elongated along latitude lines, suggesting that a transfer to zonal components is occurring. Rhines rationalized this zonal anisotropy phenomenologically by noticing that, in the later stages of the runs, weak resonant interaction theory applies as the wave steepness becomes small compared with unity. It predicts that in a wave triad energy will flow into the components of smallest frequency. In conjunction with the notion that kinetic energy still leaks to the larger scales of motion, this favours elongation of eddies along latitude lines according to the dispersion relation. The same conclusion also emerges from Plumb's (1977) analytical calculations. However the zonal anisotropy occurs readily in the initial turbulent stages and the following development aims at providing some clues to that behaviour.

The resonant theory used by the above authors describes interactions between free waves (i.e. waves satisfying the dispersion relation) and the wave steepness must be very small to offset the forced interactions. However, as nonlinearity increases, nothing guarantees that the rules governing the free and forced interactions will be the same. Moreover, it appears to be very difficult to use the resonant theory to look at the generation of zonal flows with some spatial structure because a small wave steepness (ratio of wave period to interaction time) and an infinite period are clearly irreconciliable.

In the present section we shall therefore study the 'strong' interactions of a very

limited number of Fourier components. Because of obvious mathematical limitations, one cannot provide a long term description of the interactions as in the resonant theory but only the 'small time behaviour'. Hence this is a linear stability calculation. It would not be wise to go beyond that any way within a triad configuration of Fourier components because we know that the spectral breadth of the flow will increase greatly in time at these levels of nonlinearity. In a sense the present analysis was triggered by Benjamin & Feir's (1967) study of the disintegration of wave trains on deep water, which involved consideration of off-resonance interactions.

For later comparison with the present laboratory experiments the chosen wave trio is composed specifically of a primary wave, its side band and the product of the interaction. The two important parameters guiding the discussion are the wave steepness

$$S = u|\mathbf{k}|^2/\beta$$

(where U is a r.m.s. velocity and $\mathbf{k}$ the wavenumber) and a small parameter

$$\mu = |\delta\mathbf{k}|/|\mathbf{k}|$$

describing the modulation of the primary wave of wavenumber $\mathbf{k}$ by its side band of wavenumber $\mathbf{k} \pm \delta\mathbf{k}$. The main difference of approach between the following derivation and those of Loesch and Plumb is that no *a priori* ordering of the parameters S and μ has been imposed, S being yet unspecified. Rather the outcome of the analysis will provide ranges of S as a function of μ consistent with various generations of waves longer and shorter than the primary unstable wave. The forced triad interaction equations are now derived. The conservation of potential vorticity yields the classical Rossby wave equation:

$$\nabla^2\psi_t + \beta\psi_x = -J(\psi, \nabla^2\psi), \tag{1}$$

where ψ is the stream function and J denotes the Jacobian. Solutions of (1) are sought in the triad form

$$\psi(\mathbf{x}, t) = \sum_{j=-3}^{+3} A_j(t) \exp(i\theta_j), \tag{2}$$

where

$$\theta_j = \mathbf{k}_j . \mathbf{x} - \omega_j t.$$

Moreover the conditions $A_{-j} = A_j^*$ and $\theta_{-j} = -\theta_j$ are imposed to ensure that ψ is real.

Substituting (2) into (1) and identifying Fourier coefficients on both sides such that $\theta_l + \theta_m + \theta_n = 0$ yields

$$|\mathbf{k}_n|^2 dA_n/dt = \mathbf{k}_l \times \mathbf{k}_m(|\mathbf{k}_l|^2 - |\mathbf{k}_m|^2) A_l A_m + iA_n(\beta\mathbf{k}_n . \mathbf{I} + \omega_n|\mathbf{k}_n|^2), \tag{3}$$

where $(l, m, n) = \pm(1, 2, 3)$ and two other sets obtained by permutation. $\mathbf{I}$ is a eastward unit vector. The set (3) is now used to investigate first the stability of a triad which includes components of scale larger than the primary wave. Specifically the trio consists of a primary free wave $(\mathbf{k}, \omega, A)$ which satisfies the dispersion relation, its side band $(-(\mathbf{k}+\delta\mathbf{k}), -(\omega+\delta\omega), A_s)$, and the product $(\delta\mathbf{k}, \delta\omega, A_p)$. Moreover the dispersion relation shows that to $O(\mu^2)$

$$\delta\omega = \delta\mathbf{k} . \mathbf{c}_g,$$

where $\mathbf{c}_g = \nabla_k \omega$ is the group velocity. With this choice, the set of equations (3) becomes to $O(\mu^2)$

$$\left.\begin{aligned} dA/dt &= -(\mathbf{k}\times\delta\mathbf{k})\,A_s A_p, \quad dA_s/dt = (\mathbf{k}\times\delta\mathbf{k})\,AA_p, \\ dA_p/dt &= 2(\mathbf{k}\times\delta\mathbf{k})\,\frac{\mathbf{k}.\delta\mathbf{k}}{|\delta\mathbf{k}|^2}\,A_s A + iA_p\left(\beta\frac{\delta\mathbf{k}.\mathbf{I}}{|\delta\mathbf{k}|^2}+\delta\mathbf{k}.\mathbf{c}_g\right). \end{aligned}\right\} \tag{4}$$

The system (4) is now linearized around a basic state where the amplitude of the primary wave A is much greater than A_s and A_p. The equations governing the initial tendencies of the turbulent interactions are:

$$\left.\begin{aligned} A &= A_0, \quad \frac{dA_s}{dt} = \mathbf{k}\times\delta\mathbf{k}A_0 A_p, \\ \frac{dA_p}{dt} &= 2(\mathbf{k}\times\delta\mathbf{k})\,\frac{\mathbf{k}.\delta\mathbf{k}}{|\delta\mathbf{k}|^2}\,A_0 A_s + i\Omega_p A_p, \end{aligned}\right\} \tag{5}$$

where

$$\Omega_p = \beta\delta\mathbf{k}.\mathbf{I}/|\delta\mathbf{k}|^2 + \delta\mathbf{k}.\mathbf{c}_g.$$

Looking for solutions A_s, A_p varying like $e^{i\omega t}$ yields the characteristic equation of the linear system (5):

$$\omega^2 - \omega\Omega_p + 2A_0^2|\mathbf{k}\times\delta\mathbf{k}|^2\,\mathbf{k}.\delta\mathbf{k}/|\delta\mathbf{k}|^2 = 0.$$

Hence imaginary roots and therefore instability will occur if the following condition is satisfied:

$$8A_0^2\,\frac{|\mathbf{k}\times\delta\mathbf{k}|^2}{|\delta\mathbf{k}|^2}\,\mathbf{k}.\delta\mathbf{k} > \Omega_p^2. \tag{6}$$

The first requirement is that $\mathbf{k}.\delta\mathbf{k}$ be positive. This means simply that the side band must be of a scale shorter than the primary wave for energy to be exchanged with the long wave of scale $\delta\mathbf{k}$. Assuming that this is so, one then realizes that the right-hand side of (6) is of order $|\delta\mathbf{k}|^2$ or $|\delta\mathbf{k}|^{-2}$ according to whether the long wave is zonal or not. If it is not zonal, then (6) can be simplified to

$$S^2 > G\mu^{-3} \quad \text{where} \quad S = A_0|\mathbf{k}|^3/\beta \tag{7}$$

and G is a purely geometrical factor given by

$$G = \tfrac{1}{8}\cos^2\theta/\sin^2\alpha\,|\cos\alpha|,$$

α being the angle $(\mathbf{k}, \delta\mathbf{k})$ and θ the angle between Ox and $\delta\mathbf{k}$.

The condition (7) is thus a severe one to satisfy since it requires a very large wave steepness of order $\mu^{-\frac{3}{2}}$. On the other hand, if the product of the interaction is a zonal wave, (6) becomes

$$S^2 > \tfrac{1}{2}\mu\,|\sin\phi|, \tag{8}$$

where ϕ is the angle between Ox and $\mathbf{k}$.

Hence only a small wave steepness of order $\mu^{\frac{1}{2}}$ is needed to generate a zonal flow. To be complete it is necessary to check the behaviour of triads, including waves of scales shorter than the primary component. Exactly the same kind of calculation (not reproduced here) can be applied to the group generating harmonics, namely $-(\omega, \mathbf{k})$, $-(\omega+\delta\omega, \mathbf{k}+\delta\mathbf{k})$ and $(2\omega+\delta\omega, 2\mathbf{k}+\partial\mathbf{k})$; the results follow.

For energy to be exchanged within this trio, a first necessary condition is that the

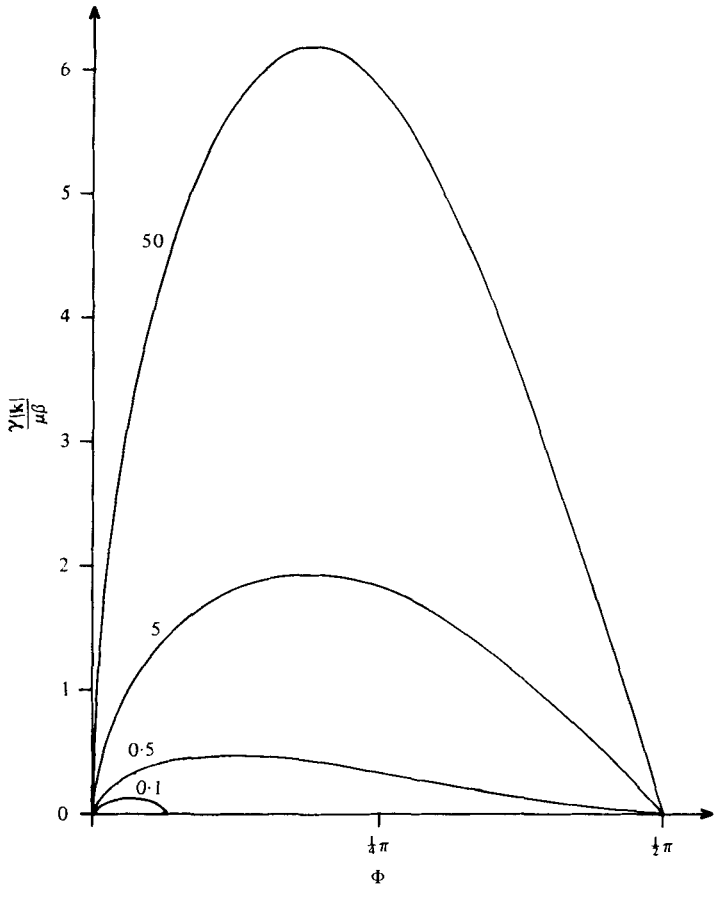

FIGURE 8. The non-dimensional growth rate as a function of the wavenumber orientation of the primary wave for several values of S^2/μ.

side-band wave must have a scale longer than the primary wave, consistent with earlier results: namely two initially small Fourier components may grow at the expense of a third, large amplitude wave if they have scale respectively shorter and longer than the latter. If so then the necessary and sufficient condition for instability, equivalent to (7) and (8), is

$$S^2 > F\mu^{-3}, \tag{9}$$

where $F = \frac{1}{4}\cos^2\phi/|\cos\alpha|\sin^2\alpha$, in which the angles have the same meaning as before.

Again very large nonlinearity is required for instability. Therefore we may conclude that, when some side-band noise is superposed on a large amplitude Rossby wave, the nonlinear interactions will force *a priori* a zonal flow at the expense of shorter-scale harmonics or longer-scale flow with non-zero meridional components. It is interesting to go back and discuss further the implications of this mechanism for

efficient zonal flow generation. In particular the growth rate γ can be computed when (8) is satisfied and one finds that

$$\gamma = \beta|\mathbf{k}|^{-1}\mu^{\frac{1}{2}}\sin^{\frac{1}{2}}\phi\,|\cos\phi|\,(2S^2-\mu\,|\sin\phi|)^{\frac{1}{2}}. \tag{10}$$

When S^2/μ is much larger than unity, the ratio of the growth rate to the frequency of the fundamental varies as $S\mu^{\frac{1}{2}}$, a value which may be significantly larger than unity, demonstrating the strength of the interaction. The orientation of the primary wave is also important. The non-dimensional growth rate has been plotted on figure 8 as a function of ϕ (the angle of the wavenumber $\mathbf{k}$ with the Ox axis) for various values of S^2/μ. For small values of S^2/μ, zonal wavenumbers (meridional crests) are favoured but the associated growth rates are small. For values of S^2/μ much larger than unity, the maximum growth rate occurs when the angle the wavenumber vector makes with Ox is 35° 2′.

It must be stressed again that the zonal flow is a forced component of low frequency $\omega_m = \delta\mathbf{k}.\mathbf{c}_g$. It is interesting to compare γ and ω_m as can be done using (10):

$$\gamma/\omega_m = \tfrac{1}{2}(2S^2/\mu\,|\sin\phi| - 1)^{\frac{1}{2}}.$$

The magnitude of this ratio is large when S^2 exceeds μ, this being also favoured by a more meridional orientation of the wave crests. Thus in this limit the strength of the zonal flow builds up quickly before it has completed a single slow oscillation. It is really in this sense that this mechanism can be recognized as an efficient but transient way to build up a mean zonal flow.

The main difference of approach of the present calculation from those using weak resonant interaction theory is that we have not imposed *a priori* that the wave steepness be small. Rather we have shown that, by increasing gradually the wave steepness of a slowly modulated primary plane wave, a zonal flow will be forced at first (when S becomes larger than $\mu^{\frac{1}{2}}$, and on a sufficiently short time scale to make the mechanism a realistic one. Of course we must stress again that the forced zonal flow does not have zero frequency but rather is modulated on a long time scale. It is, however, quasi-steady because the time scale of growth is so much shorter than the modulation time scale as soon as S exceeds $\mu^{\frac{1}{2}}$), itself small compared with unity. As in any stability analysis, the calculation shown here indicates only the initial tendency of the behaviour of a turbulent triad and not the complete temporal evolution provided by weak resonant theory. Here the mechanism favouring the zonal flow is one of amplitude selection among forced components. This contrasts greatly with weak resonant theory, which favours reversible energy transfer among triads of free waves obeying a 'phase' relationship. In that theory the forced interactions that we have considered here are much smaller than the free interactions because of the small wave steepness hypothesis (Longuet-Higgins & Gill 1967)†. Of immediate concern should be the extension of the present theory to the continuous case, in which the evolution of a narrowly peaked spectrum of turbulence would be looked at. In particular one would like to see how the growth rate for the zonal flow would depend upon the height and width of the initial spectrum.

† See note added in proof on p. 64.

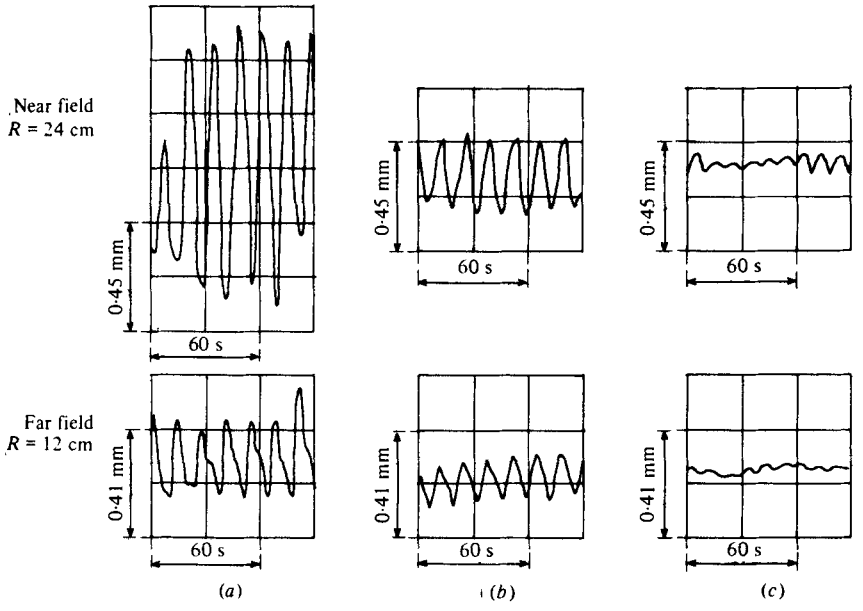

FIGURE 9. Pressure time series when: (*a*) the driving moves westward (retrograde); (*b*) the driving moves eastward (prograde); (*c*) the driving is stationary.

5. Experimental signature of the dynamics

This section provides several links between specific measurements of the flow and theoretical predictions based upon quasigeostrophic theory. It has been shown by Colin de Verdière (1977) that, when the Rossby and Ekman numbers, the forcing vertical velocity and frequency are all at most of the order of the topographic slope (itself smaller than unity), a consistent perturbation expansion of the fields in powers of that slope leads at zeroth order to geostrophy and at first order to the following potential vorticity equation, valid for a fluid with a free surface:

$$\left[\frac{\partial}{\partial t}+J(\psi)\ldots\right]\nabla^2\psi-\frac{f}{H}\nabla H.\mathbf{k}\times\nabla\psi-\frac{1}{\lambda^2}\frac{\partial\psi}{\partial t}=-R\nabla^2\psi+\nu\nabla^4\psi-\frac{f}{H}w_B, \qquad (11)$$

where ψ is the stream function, ν the kinematic viscosity, H the mean depth and w_B the vertical velocity imposed at the bottom. Also, $E=\nu/\Omega H^2$ is the Ekman number, $R=\Omega E^{\frac{1}{2}}$ is the inverse of the Ekman spin-up time and $\lambda=(gH)^{\frac{1}{2}}/f$ is the external Rossby radius of deformation. In the following subsections, various approximations of (11) will be used to extract simple dynamical statements which may be checked experimentally.

5.1. *Wave resonance and wave stresses*

With closed geostrophic contours provided by the paraboloidal shape of the free surface, the first effect to check concerned the selective amplification of the waves when the driving of the zonally travelling wave moved either eastward or westward. The difference was indeed striking. The well-ordered steady waves found in the retrograde case (figures 3 and 6) were replaced by quite an unsteady messy pattern when the forcing moved in a prograde sense, showing that the fluid did not respond favourably

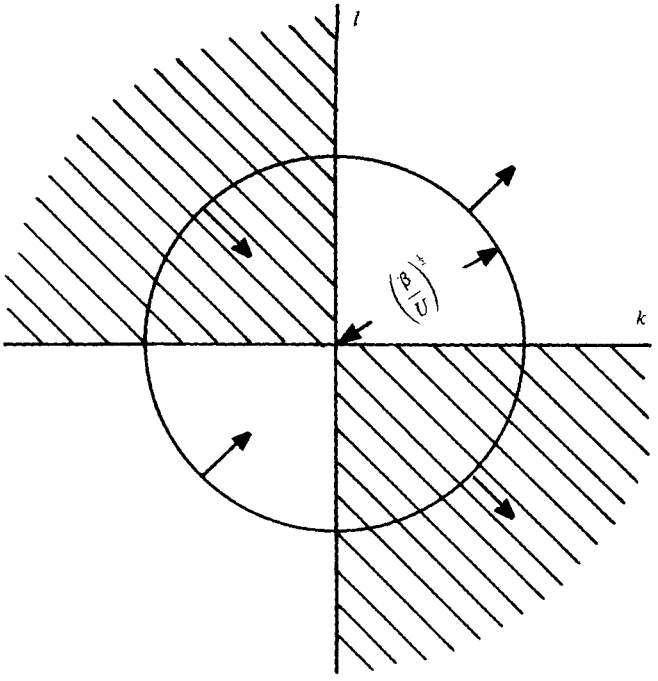

FIGURE 10. Locus of wavenumbers which may be excited under the action of a westward-travelling disturbance. Arrows represent the group velocity relative to the forcing.

to such excitation. To give a quantitative estimate of the difference, pressure time series from two capacitance probes in the near and far field were obtained and are shown on figure 9. With a wave steepness of order unity, the enhancement of the signal for the retrograde case demonstrates quite clearly the necessity for the direction of propagation of the forcing to match the direction of the Rossby wave phase speed in order that significant motions be produced. For smaller forcing amplitudes the signal corresponding to the prograde case looked exceedingly small. Another simple aspect of linear theory which could be investigated easily concerns the orientation of the wave crests away from the directly forced region. Lighthill (1967) demonstrates that travelling forcing effects generate waves whose crests are stationary relative to the forcing. They will be found in the direction of the group velocity (relative to the forcing) with wavenumbers satisfying (within the classical β-plane equations)

$$-\beta k/(k^2+l^2) = -kU, \quad U > 0,$$

k and l being the zonal and meridional wavenumber respectively. Thus the possible wavenumbers may lie on the l axis and on a circle of radius $(\beta/U)^{\frac{1}{2}}$ centred at the origin. The former family, with zero zonal wavenumber, will not be excited because our forcing spectrum has no energy there. On the other hand, wavenumbers lying on the circle will be actively generated. In figure 10 this locus has been plotted *vs.* the direction of the group velocity. Since in our experiments the forcing is bounded to the south by a rigid wall, the northern interior will be filled by waves with wavenumbers lying in the first and third quadrant of figure 10 exclusively. This indicates in turn a northwest–southeast orientation of the wave crests. Long exposure photographs

over one forcing period were taken at a very small amplitude level (steepness = 0·2) so that particle paths were essentially closed. Figure 11 (plate 3) reveals the elliptical orbits with orientation deduced from the theory. One may also see that the size of the loops decreases northwards because of the usual energy decay away from a source. These two effects, orientation and varying size of the orbits, are the necessary ingredients to produce positive divergence of the wave-induced Reynolds stresses. The meridional distribution of $\overline{u'v'}$ in figure 4(*a*) displays the same information but for more energetic driving. As can be observed in figure 11 some particles closer to the forcing are already trapped by this rectified westward circulation.

There is a second type of resonance concerned with whether or not the waves feel the presence of the boundaries. Although the high mode structure chosen has a scale smaller than the dimensions of the basin it is to be expected that minimizing frictional effects, as explained earlier, will enable wave resonance to show up, allowing the experimental determination of the frequencies of the inviscid Rossby modes. In a cylindrical geometry with a free-surface height varying like $\Omega^2 r^2/2g$, the linearized version of (11) becomes

$$\frac{\partial}{\partial t}\left(\nabla^2\psi - \frac{\psi}{\lambda^2}\right) + \frac{\psi\theta}{4\lambda^2} = -\epsilon\nabla^2\psi - \frac{w_B}{H}, \tag{12}$$

where time has been non-dimensionalized by the Coriolis parameter and $\epsilon = R/f$. This is to be solved with the auxilliary boundary condition that $\psi = 0$ at $r = a$. In (12), lateral friction has been omitted. The present analysis is not concerned with the role of the Stewartson layers required to bring the velocity to zero at a solid wall. Simple scale analysis shows that away from those boundary layers Ekman friction will exceed lateral friction if, as in the present experiment, the scale of the wave is greater than $HE^{\frac{1}{2}}$.

The inviscid free normal modes of the vorticity equation (12) are:

$$\psi_{nm} = J_n(\eta_m r/a)\exp\left[i(\omega t + n\theta)\right]$$

where J_n is the nth-order Bessel function of the first kind and η_m its mth zero. The corresponding dispersion relation is

$$\omega_m = n/4[1 + (\eta_m \lambda/a)^2].$$

As usual it associates large frequencies with large meridional scales (small η_m). The radial equation derived from (12) has a turning point, thus the radial envelope of the normal mode J_n changes its nature according as its argument is smaller or larger than n. Thus when r is greater than $r_c = an/\eta_m$, the Bessel function has an oscillatory character, while for smaller values of r it decays algebraically to zero. This corresponds physically to the fact that it is impossible for a wave packet starting from the outer wall to reach the centre. As it moves into shallower water, with β decreasing linearly, its meridional scale must increase. This augments and bends the group velocity eastwards until the packet is essentially reflected at a critical latitude, limiting thereby further meridional penetration of energy.

To compare experimental resonance with theory, the following forcing function was chosen:

$$W = W_0 \frac{\delta(r - r_0)}{r} \exp\left[i(\omega t + n\theta)\right].$$

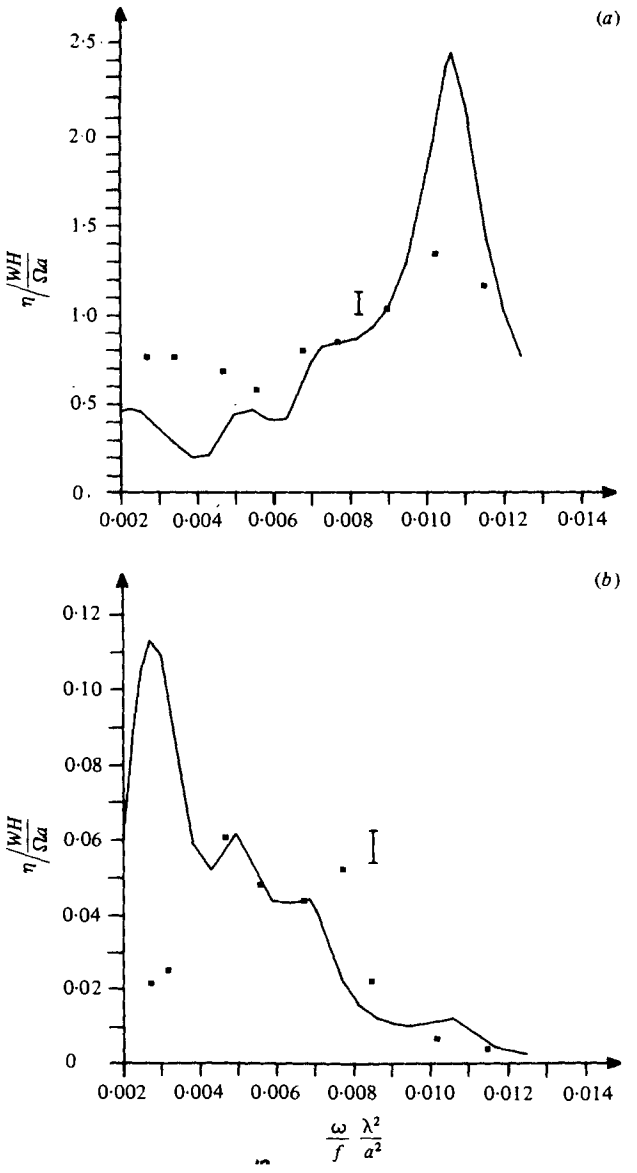

FIGURE 12. The resonance curves: ——, theory; ■, experimental values. (*a*) The near field; $R = 24$ cm, (*b*) The far field; $R = 12$ cm; η represents the measured crest-to-trough wave amplitude in cm.

The radial part is idealized by a Dirac δ function rather than a more distributed function as in the experiments. The travelling wave is assumed to be harmonic in time although a square wave was forced in the experiments. These two idealizations have some important consequences when dealing with waves of finite steepness. The steadily forced solution is found by expanding the forcing over the normal modes. The non-dimensional result is:

$$\psi = \mathscr{R}\left[\exp\left[i(\omega t + n\theta)\right] \sum_{m=1}^{\infty} \frac{[i(\omega-\omega_m)-\epsilon]}{[(\omega-\omega_m)^2+\epsilon^2]} \frac{J_n(\eta_m r_0/a)\, J_n(\eta_m r/a)}{\eta_m^2 [J_{n+1}(\eta_m)]^2}\right], \tag{13}$$

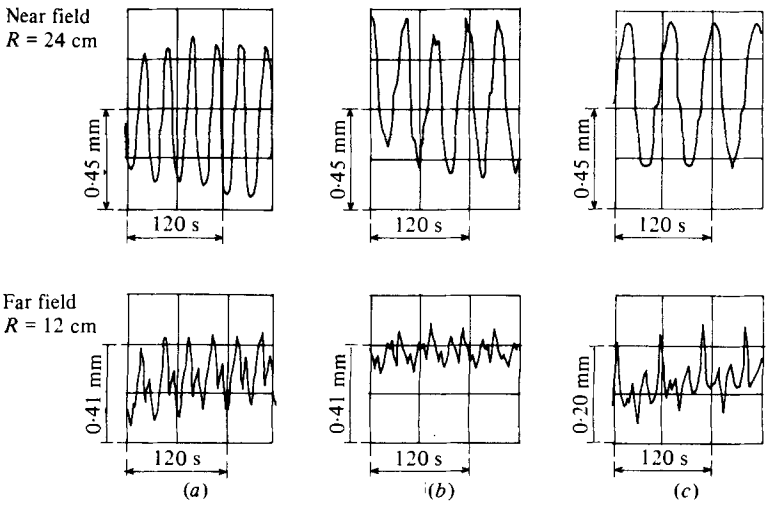

FIGURE 13. Pressure time series for three distinct frequencies of excitation: (*a*) = 0·216 rad/s; (*b*) = 0·167 rad/s; (*c*) = 0·124 rad/s. Other parameters which were held fixed are: Ω = 3·7 rad/s; H = 9 cm; Q = 300 cm^3/s.

in which the approximation $a/\eta_m\lambda \ll 1$ has been made. This is valid for comparison with our experiments because a/λ never exceeds 2 or 3 and the smallest value of η_m is 16·70 for the mode number 12. The easiest check to see if the solution (13) corresponds to the experiment is to measure the free-surface elevation as a function of time and compare the r.m.s. pressure with the theoretical amplitude. We shall sweep over a range of frequencies for gentle driving. There is however an unknown adjustable parameter: the forcing amplitude W_0. Although the mass flux is known, there are no direct ways of inferring the vertical velocity because the effective area of sources and sinks covered by a diffuser is essentially unknown. Instead the present comparison provides a way of estimating W_0 at a given frequency. The value so obtained was then used to scale the data at other frequencies. The pressure was measured using capacitance probes at two points in the tank, one in the near field (r = 24 cm) and one in the far field (r = 12 cm). Because the pressure signal associated with quasi-non-divergent Rossby waves is very small we could not go as low in forcing amplitude as is required by the linear theory. The smallest free-surface elevation that we could detect with a good signal-to-noise ratio was about 50 μm. This corresponded to a Rossby number of order 10^{-2} but a wave steepness still of order 0·5 for the gravest Rossby modes. Figure 12 shows the comparison between experimental data and the theoretical curves computed from (13). (The value of the spin-up time used in the theoretical solution was measured *in situ*. It varied as $T = 0{\cdot}75H/(\nu\Omega)^{\frac{1}{2}}$, which is 25% lower than the theoretical value.) Qualitative agreement exists: the lowest mode is slightly resonant in the near field as indicated by the peak at ω = 0·0105. Moreover the presence of β critical latitudes is well demonstrated as the driving frequency must be below a certain cut-off for any wave energy to reach the far-field probe (as shown on figure 12(*b*)). However the theoretical curves look sharper and the comparison deteriorates at low frequencies as nonlinearity creeps in. The modelling of the driving as a zonal sine wave and the finite steepness of the experimental waves are probably both important factors explaining the different widths of the spectra. At any rate both

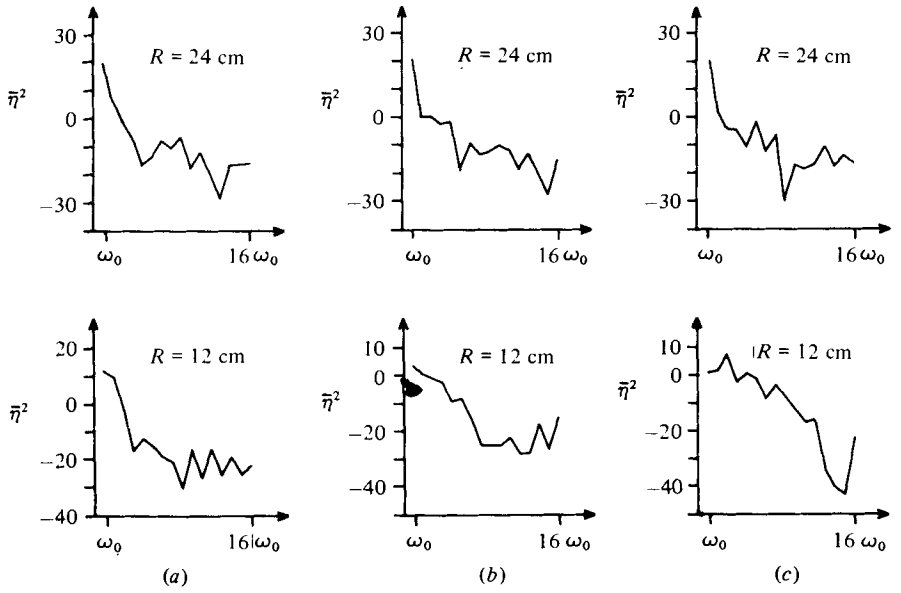

FIGURE 14. The autospectra of the pressure time series shown in figure 13; ω_0 is the frequency of the primary wave. (*a*) ω = 0·216 rad/s; (*b*) ω = 0·167 rad/s; (*c*) ω = 0·124 rad/s.

the theoretical and experimental curves indicate that only the highest frequency mode feels the size of the container because of important Ekman damping.

A few observations were obtained at higher amplitude levels with the Rossby number five times larger. They indicate an important spectral broadening of the empirical curves and also that more and more energy could tunnel through the critical latitude when the driving frequency was above the 'linear low frequency cut-off'.

This paragraph deals with certain finite amplitude effects of the Rossby waves as revealed by pressure time series. Several runs with a constant large forcing amplitude and decreasing frequency were made. Wave forms and their spectra are shown on figures 13 and 14 respectively. The observation that the second and third harmonic occur at a fixed point on the back of the primary wave train suggests that they travel at the same phase velocity as the basic wave. This indicates that we are dealing with a genuine manifestation of nonlinear interactions of the primary wave. The disintegration of the primary wave as it travels away increases as the wave frequency decreases. This is clearly what the spectra of figure 14 indicate. This is not surprising: the number of possible nonlinear interactions of the primary wave as it moves from the forced region to the far field varies like the ratio of the energy propagation time to the nonlinear interaction time. The former varies like the inverse of the group velocity and thus increases at lower frequencies. The latter varies like wavelength divided by particle speed and thus decreases with frequency. Hence lowering the driving frequency will make the nonlinear energy transfer between Fourier components more complete. It is interesting to know the order of magnitude of the wave steepness when second harmonics have just appeared, as in figure 13(*a*). By measuring the particle velocity at this forcing strength the steepness (equal to U'/c) turns out to be about 6·0. On the other hand, as can be seen from figure 5, we have positive indications that for a wave steepness as low as 0·4 measurable zonal flows could be detected.

Therefore the experiments suggest that nonlinearities needed to generate harmonics are 15 times greater than those inducing zonal flows. Because of engineering considerations the frequency spectrum of the driving is not a line spectrum but possesses some side-band energy around the fundamental. The experimental result is thus reminiscent of the stability theory of §4, in which it was found that a zonal flow is generated faster and at 'lower amplitude levels' than waves of longer or shorter scale generated by turbulent interaction between a large primary wave and its side bands. Although dissipation, forcing and unequal beta are all complicating influences which must be further evaluated, the above results suggest that the amplitude thresholds found in the theory are qualitatively correct.

5.2. *Connexion with potential-vorticity mixing theory*

As figure 5 shows, the present experiment demonstrates that the zonal flows spontaneously appearing on a beta plane are driven by the eddies. Specifying mean flow accelerations as divergences of Reynolds stresses is of limited informative value. It does not reveal the whole of the physical nature of the rectification processes. The novelty of a vorticity mixing approach is that it allows one to disentangle the free and forced contributions to the potential-vorticity fluxes. Although what one can say about forced regions is at present limited, considerable intuition is available to predict mean flows at the 'unforced latitudes' of a beta plane with closed contours as shown by Rhines (1977). The vorticity mixing theory derived below is a slightly modified version of Rhines's. On a non-divergent, beta plane with Ekman friction the vorticity equation can be rewritten as

$$(D/Dt+R)\,q = R\beta y + F, \tag{14}$$

where D/Dt denotes the Lagrangian derivative, R the friction coefficient and F a forcing function. The potential vorticity is $q = \xi + \beta y$. The zonally averaged complete x momentum equation may be manipulated to yield

$$(\partial/\partial t + R)\,\overline{u} = \overline{qv}, \tag{15}$$

where it has been assumed that the zonal average of the function whose curl is F is zero. To obtain a simple expression for the meridional transport of potential vorticity one may construct the time integral of (14) following a fluid parcel which had potential vorticity q_0 at latitude y_0 and time $t = 0$. Hence at a later time t and a latitude y the potential vorticity is

$$q = q_0 e^{-Rt} + R\beta \int_0^t y(t') \exp\left[R(t'-t)\right] dt' + \int_0^t F(x(t'), y(t'), t') \exp\left[R(t'-t)\right] dt'.$$

Zonally averaging the meridional flux qv about this fixed latitude γ at time t yields

$$\overline{qv} = \overline{q_0 v} e^{-Rt} - R\beta \int_0^t \exp\left[R(t'-t)\right] \int_0^{t-t'} R_{22}(\tau)\, d\tau\, dt' + \int_0^t \overline{V(y,t)\, F(x(t'), y(t'), t')} \exp\left[R(t'-t)\right] dt', \tag{16}$$

where $R_{22}(\tau) = \overline{v(t)\, v(t-\tau)}$ is the Lagrangian autocorrelation in the meridional direction. The north–south diffusitivity of fluid parcels observed at latitude y and t which at a prior time t' were at y', can thus be written as

$$K_{22}(t-t') = \frac{1}{2} \overline{\frac{D}{Dt} (y-y')^2} = \int_0^{t-t'} R_{22}(\tau)\, d\tau.$$

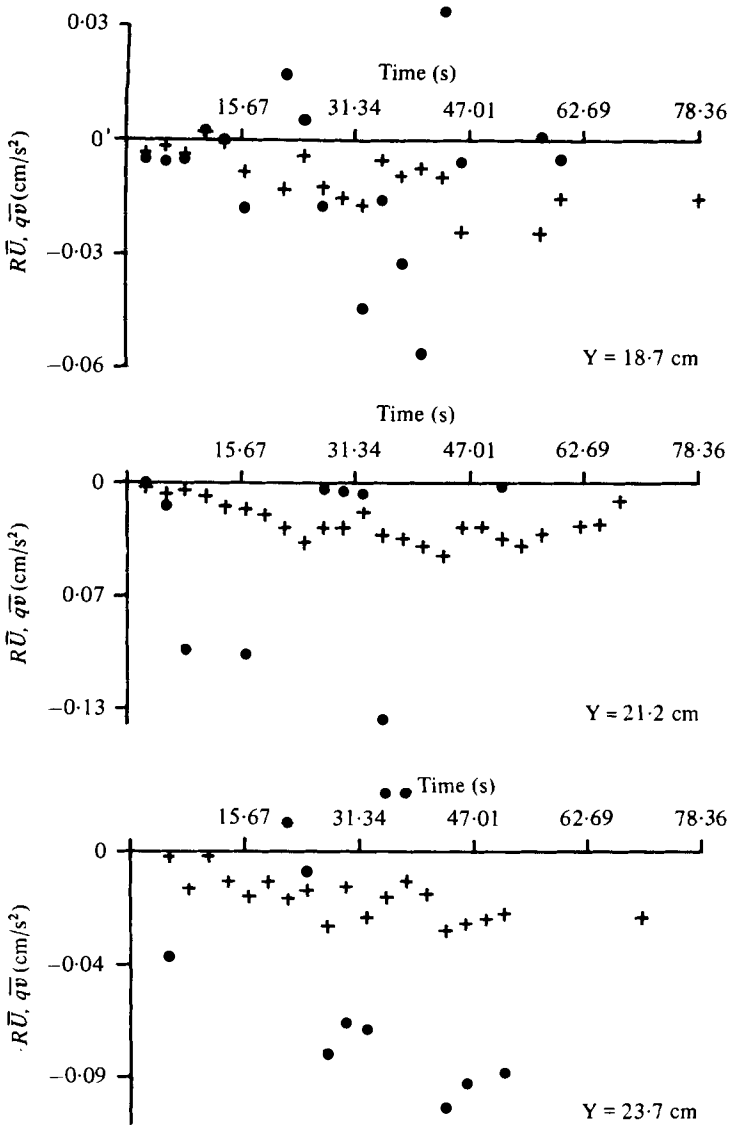

FIGURE 15. Experimental comparison of mean flow acceleration and potential vorticity flux at free latitudes in the transient stages. The forcing was impulsively turned on at the time origin. Laboratory parameter values are: $\Omega = 4{\cdot}05$ rad/s; $\omega = 0{\cdot}442$ rad/s; $Q = 360$ cm³/s; $H = 7$ cm. +, $R\bar{U}$; ●, $\overline{qv}$.

In (16) the first term represents the viscous spin-down of the initial transport of potential vorticity by the eddies and can be expressed as

$$\overline{q_0 v} = \overline{\xi_0 v} - \beta K_{22}(t).$$

Substituting these terms back into (15) gives

$$\overline{qv} = \overline{\xi_0 v}\, e^{-Rt} - \beta K_{22}(t)\, e^{-Rt} - R\beta \int_0^t K_{22}(\tau)\, e^{-R\tau} d\tau + \int_0^t \overline{VF} \exp\left[R(t'-t)\right] dt'. \tag{17}$$

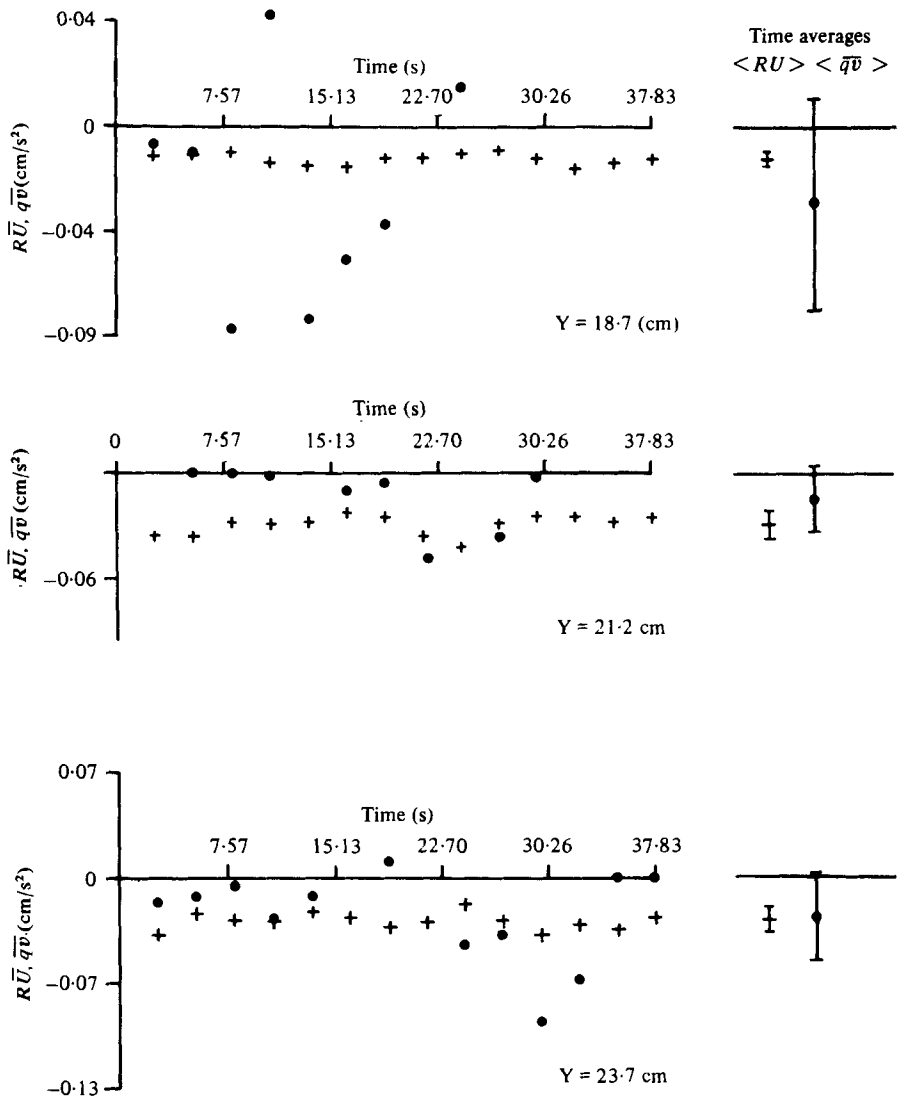

FIGURE 16. Experimental comparison of mean flow acceleration and potential vorticity flux at free latitudes in the statistically steady state. Laboratory parameter values and symbols as in figure 15.

The relation (17), valid for finite amplitude motions, is a powerful one. Consider exciting a fluid on a β plane, at rest initially, by some remote forcing action; then at these distant free latitudes, (17) predicts that westward accelerations occur in the transient and steady state from the second and third terms in (17). This is so because in a continuously forced fluid, the diffusivity $K_{22}(t)$ is positive. Thus westward currents develop in free regions as a result of an irreversible mixing of the gradient of planetary vorticity. Because no net momentum may appear in the fluid, eastward currents must also be found in the forced regions. This implies that the last term in (17) has to be positive there. However at present the precise way in which this can occur remains unclear.

The experiments described earlier fit neatly into this description. More quantitative comparisons can be provided. The first makes use of figure 5 which shows that, in the steady state, the zonally averaged westward current scales with neither v' nor $\overline{v'^2}$ but somewhere in between. The third term in (16), a weighted integral of the diffusivity, indicates just that.

The second comparison involves more detailed measurements: it was decided to check directly from the observations if the magnitude of the westward mean flow finally equilibrates to

$$\beta \int_0^t K_{22}(\tau)\, e^{-R\tau} d\tau, \quad Rt \gg 1,$$

at free latitudes as it should in the statistically steady state on the basis of (17). A number of Lagrangian particle paths were extracted from ciné-films and digitized. Fixes of the trajectories were taken roughly every fifth of a wave period. Typically around 700 fixes were spread over a spin up time scale. As shown by the above expression the steady state value of the potential vorticity flux necessitates only a knowledge of the zonally averaged meridional diffusivity K_{22} and of the spin-up time. At any given time and latitude, a large number of fluid parcels just crossing the line is needed for constructing meaningful zonal averages of Lagrangian statistics. This was a hard requirement to satisfy. To increase the number of degrees of freedom, the zonal average was applied to a narrow latitude band rather than to a line as in (17). Having the set of trajectories at hand, K_{22} was numerically evaluated in the following way: for a given band and time, particles lying within the band were identified. This set of particles was followed backwards in time and Lagrangian velocity correlation were computed by averaging over the set, usually made of between 5 and 15 particles.

The number of degrees of freedom is not very large in spite of the large amount of data input. This explains certainly most of the noisy behaviour of the estimates. The diffusivity was obtained by integrating the correlation in time. Note that such a computation actually estimates the backward diffusivity used in the theory. Bearing in mind these limitations, the results of such free latitude computations are shown on figures 15 and 16. They depict the value of the frictional force and of the statistically steady $\overline{qv}$. Thus in the long run these two quantities should equilibrate. Figure 15 represents such a calculation for the transient stages, immediately after switch-on. One may note that the high degree of scatter in the potential vorticity fluxes prevents documentation statistically of such an equilibration. However on the whole, the negative sign of the fluxes seems to occur, indicating that a down gradient mixing of potential vorticity is occurring. Such computations carried out when the flow has reached a statistically steady state are shown on figure 16. The scatter is less because stationarity could be used to increase the degrees of freedom. On the right side of the graph the time-averaged values and standard deviation of all data points have been plotted. These results are suggestive of a gross agreement (only) with the voriticity mixing theory and no pretension has been put forward that this case is statistically significant. Although the wave steepnesses are order one, the turbulence is not very diffusive and particles do not wander very far in latitude. Thus the long-term meridional dispersion is bounded, which implies that the long-term diffusivity vanishes. Clearly the β effect introduces a strong meridional restoring force.

Somewhat aside from the preceding discussion, an *a priori* puzzling fact can be

observed in figure 6. Indeed it is realized that cyclonic eddies at forcing latitudes are so much enhanced compared with anticyclonic ones that the latter almost disappear. Now the retrograde sense of the interior mean flow is evidently just what is needed to intensify cyclones and weaken anticyclones at the forcing latitudes. The beta effect, therefore, introduces an asymmetry in the eddy pattern; the anticyclones grow preferentially to a larger scale (to form the interior westward mean flow) while cyclones stay at smaller scales tied up to the directly driven southern region. Thus one may say that in this context the spectral characteristics of the eddies depend upon the sign of pressure anomalies. A control run was carried out by performing the same experiment but replacing the upper paraboloidal surface by a rigid flat lid. In the transient stage on this f plane, initially small eddies exhibited the usual tendency to grow to larger scales 'irrespective of their signs' as in classical two-dimensional turbulence and no organized mean flow could be detected. One must not infer from the β-plane runs, however, that a meridional vorticity partition is associated with the distribution of the eddies. Contrasting this with geostrophic turbulence over bumpy topography, one may show that the 'area-averaged' $\overline{\xi r}$ correlation (where ξ is the relative vorticity) vanishes after taking into account the axial symmetry of the forcing.

5.3. *The spin-down period*

The observations were presented briefly in § 3. 'Total area' averaging of mean and eddy velocity fields indicated a tendency for eddy kinetic energy (respectively mean kinetic energy) to spin down at a faster rate (respectively slower) rate than the Ekman dissipation time scale. These results shown in figure 7, therefore indicates that the mean flow is stable to finite amplitude smaller scale perturbations. One could argue, however, that the strong damping of the waves whose energy peaks in the forced region might be due to uneven bottom roughness in this region compared with the interior as shown by figure 1. Controlled experiments reveal that the spin-up time scale decreased by about 30 % when the smooth bottom has been covered by a rougher sheet of foam rubber. This reduction is not sufficient to account for the observations, which show that the initial decrease of eddy kinetic energy occurs on the inertial time scale, which is really an order of magnitude smaller than the viscous time scale. The role played by lateral friction seems to be equally minor: for scales as small as 1 cm (i.e. a tenth of the eddy energy containing scale) the associated lateral decay time of the order of 100 s is far too long to matter.

Recalling the existence of two integral invariants of the motions, these energy redistributions are not surprising; indeed on an unblocked beta-plane, total kinetic energy and relative enstrophy are conserved. It is then possible to show that nonlinear interactions in freely decaying turbulence lead to an expansion of the energy-containing scale. The energy migration observed here from the short waves to the larger-scale mean flow is after all just following that rule.

Hydrodynamic stability theory can only with extreme difficulty produce such general results and it is customary to make case studies of selected, usually inviscid mean flows. Whether classical stability studies are as useful as initial-value problems to explore the physical mechanisms of wave/mean-flow interaction problems remains to be seen. One may, however, recall some of the conclusions of the former in the present context. For inviscid flow self-excited and damped perturbations, being

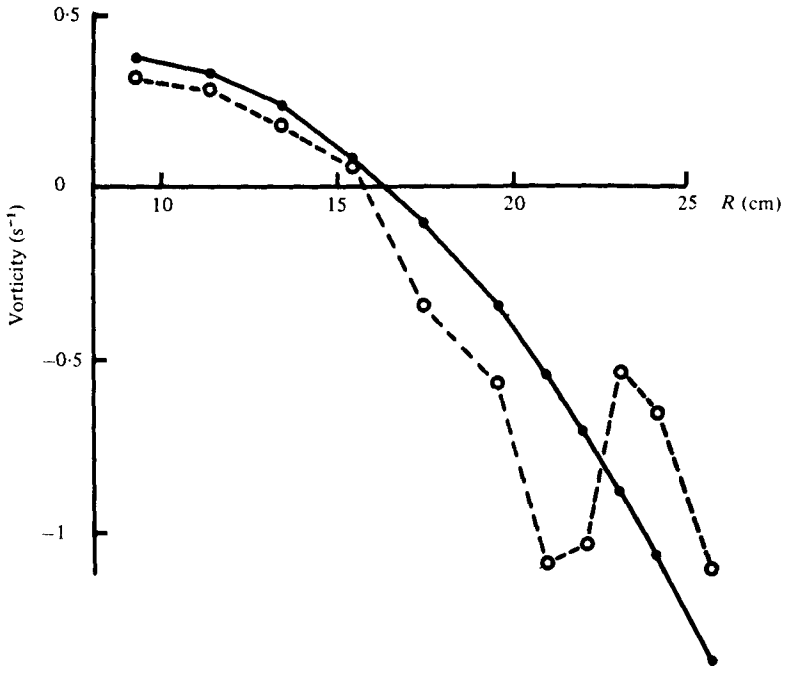

FIGURE 17. Experimental values of potential vorticity as a function of radial distance for a run as in figure 6(*a*) (plate 2). ●, planetary vorticity; ○, absolute vorticity.

complex conjugates, coexist. This clearly restricts the usefulness of the theory to the self-excited case. In connexion with the shear waves embedded in the atmospheric westerlies, Kuo (1949) showed that a necessary condition for a zonal flow to be unstable on a β-plane is that the gradient of mean potential vorticity vanishes somewhere. If this is so, one may adapt Lin's (1955) result to show that unstable solutions exist in the neighbourhood of the neutral curve. In the event that the function $k(y) = (U-c)^{-1}dQ/dy$ remains positive (U being the zonal flow, c the phase speed of the perturbations and Q the mean potential vorticity), one deduces that instability will occur for waves with scales longer than neutral. This argument applies well to a broad class of westward flows but went almost unnoticed because $k(y)$ never keeps the same sign for westerlies. This is about as far as one can go within the framework of inviscid theory. The relevance to the above experimental observations is weak. Indeed Kuo's criterion has been plotted on figure 17 for the large amplitude run corresponding to figure 6(*a*). Extrema of mean potential vorticity are found near the maximum of the westward jet and, as we recall, the waves are damped. Furthermore smaller amplitude runs producing weaker zonal flows do not yield extrema in the meridional distribution of potential vorticity. In these cases also, however, the damping of the perturbations occurred on the inertial time scale whereas the application of inviscid theory would predict no energy exchange between waves and the mean flow. Thus Kuo's criterion has probably little to do with the existence of exclusively damped solutions. Clearly the theory must accommodate other effects such as time dependence or viscosity.

6. Conclusion

We have shown both experimentally and theoretically that finite amplitude Rossby waves are fully capable of exciting mean flows along geostrophic contours when the latter are not blocked by obstacles or meridional boundaries. The occurrence of westward jets away from forced regions seems to be reasonably explained by a down-gradient mixing of potential vorticity. However more work needs to be done to elucidate the behaviour of flow-forcing velocity correlation.

The direct relevance to atmospheric planetary motions might be important because the geostrophic contours are 'unblocked' in both geometries. Although the thermal forcing induces directly a strong mean circulation which might obscure genuine rectification processes, the above results should prompt one to look for long-term sources and sinks of mesoscale energy. These must be correlated with anomalies of the directly driven zonal circulation schemes. In the meantime, to make accurate predictions of the sign of the anomalies (for instance the mid-latitude surface westerlies), the influence of density stratification upon the rectified circulation schemes presented here must be evaluated.

Further model studies are needed to explore the connexions with the oceanic circulation. In particular the influence of meridional boundaries must be carefully assessed along the lines initially explored by Pedlosky (1965). At this time the present work suggests caution when neglecting the effect of these eddy-vorticity fluxes in model or diagnostic studies of the general circulation. This is clearly supported by the abundant evidence of the overwhelming eddy activity in the world oceans and also by recent observations (Worthington 1977; Schmitz 1977) which indicate smaller-scale mean gyres in the western North Atlantic than were previously expected on the basis of exclusively wind-driven circulation models.

Throughout the course of this work the author benefited greatly from numerous discussions with Dr P. B. Rhines. The original design of the experiment was put forward by Dr A. McEwan and his help is gratefully acknowledged here. Part of this paper originates from a doctoral thesis submitted by the author at the Massachusetts Institute of Technology and the Woods Hole Oceanographic Institution. Support was provided by the National Science Foundation under grant OCE 75-21674. The author is also very much indebted to Mrs M. Beuzart for typing the manuscript and to M. J. Kervella for plotting the figures. This is Woods Hole Oceanographic Institution contribution no. 4282.

REFERENCES

BEARDSLEY, R. C. 1969 A laboratory model of the wind driven ocean circulation. *J. Fluid Mech.* **38**, 255–271.

BEARDSLEY, R. C. 1975 The sliced cylinder laboratory model of the wind driven ocean circulation. Part 2. Oscillatory forcing and Rossby wave resonance. *J. Fluid Mech.* **69**, 41–64.

BENJAMIN, T. & FEIR, J. 1967 The disintegration of wave trains on deep water. *J. Fluid Mech.* **27**, 417–430.

COLIN DE VERDIÈRE, A. 1977 Quasigeostrophic flows and turbulence in a rotating homogeneous fluid. Ph.D. thesis, Mass. Inst. of Tech., Cambridge and Woods Hole Ocean. Inst.

KUO, H. 1949 Dynamic instability of two-dimensional non-divergent flow in a barotropic atmosphere. *J. Met.* **6**, 105–122.

LIGHTHILL, M. J. 1967 On waves generated in dispersive systems by travelling forcing effects, with applications to the dynamics of rotating fluids. *J. Fluid Mech.* **27**, 725–752.

LIN, C. C. 1955 *Theory of Hydrodynamic Stability*. Cambridge University Press.

LOESCH, A. Z. 1977 On generation of zonal flows by interacting Rossby waves. *Tellus* **29**, 306–316.

LONGUET-HIGGINS, M. S. & GILL, A. E. 1967 Resonant interactions between planetary waves. *Proc. Roy. Soc.* A **299**, 120–140.

NEWELL, A. C. 1969 Rossby wave packet interactions. *J. Fluid Mech.* **35**, 255–271.

PEDLOSKY, J. 1965 A study of the time dependent ocean circulation. *J. Atmos. Sci.* **22**, 267–272.

PHILLIPS, N. A. & IBBETSON, A. 1967 Some laboratory experiments on Rossby waves with application to the ocean. *Tellus* **19**, 81–88.

PLUMB, R. A. 1977 The stability of small amplitude Rossby waves in a channel. *J. Fluid Mech.* **80**, 705–720.

RHINES, P. B. 1975 Waves and turbulence on a beta-plane. *J. Fluid Mech.* **69**, 417–443.

RHINES, P. B. 1977 Dynamics of unsteady currents. *The Sea*, vol. 6. Wiley.

SCHMITZ, W. J. 1977 On the deep general circulation in the western north Atlantic. *J. Mar. Res.* **35**, 21–28.

STARR, V. P. 1968 *Physics of Negative Viscosity Phenomena*. McGraw-Hill.

STOMMEL, H. 1948 The westward intensification of wind driven ocean currents. *Trans. Am. Geophys. Un.* **29**, 202–206.

THOMPSON, R. 1971 Topographic Rossby waves at a site north of the Gulf Stream. *Deep-Sea Res.* **18**, 1–19.

WHITEHEAD, J. A. 1975 Mean flow driven by circulation in a beta-plane. *Tellus*, **27**, 358–364.

WORTHINGTON, V. 1977 On the north Atlantic circulation. *Johns Hopkins Ocean. Stud.*, no. 6. Johns Hopkins University Press.

Note added in proof (26 February 1979)

The different domains of application may be further substantiated. As pointed out earlier by Rhines (1975) a resonant interaction mechanism may favour 'nearly zonal' flows. A referee has pointed out that this result can be recovered easily within the present formulation. If one considers a triad composed of a primary wave, its sideband and a long wave, the latter must satisfy the dispersion relation. This implies that Ω_p in (6) must go to 0. As a consequence, the threshold requirement drops out, i.e. the long wave may be generated at arbitrarily small wave steepness. It remains to see what is the preferred orientation of this wave. The possible wavenumbers are to be found on the resonance curve whose equation is given by: $\Omega_p = 0$. That is

$$\delta k = \frac{2kl}{k^2 + l^2} (\delta l)^3.$$

This is the asymptotic version near the origin of Longuet-Higgins and Gill's full resonance curve. This shows that nearly zonal flows ($\delta k/(\delta l)^3 = O(1)$) are in fact produced by resonant interaction. The growth rates are identical with those derived earlier for the non-resonant case when S is much larger than $\mu^{\frac{1}{2}}$.

The conjunction of both resonant and non-resonant mechanism therefore indicates that if a Rossby wave of small or large steepness is modulated, it will always be accompanied by quasi-steady zonal or nearly zonal waves.

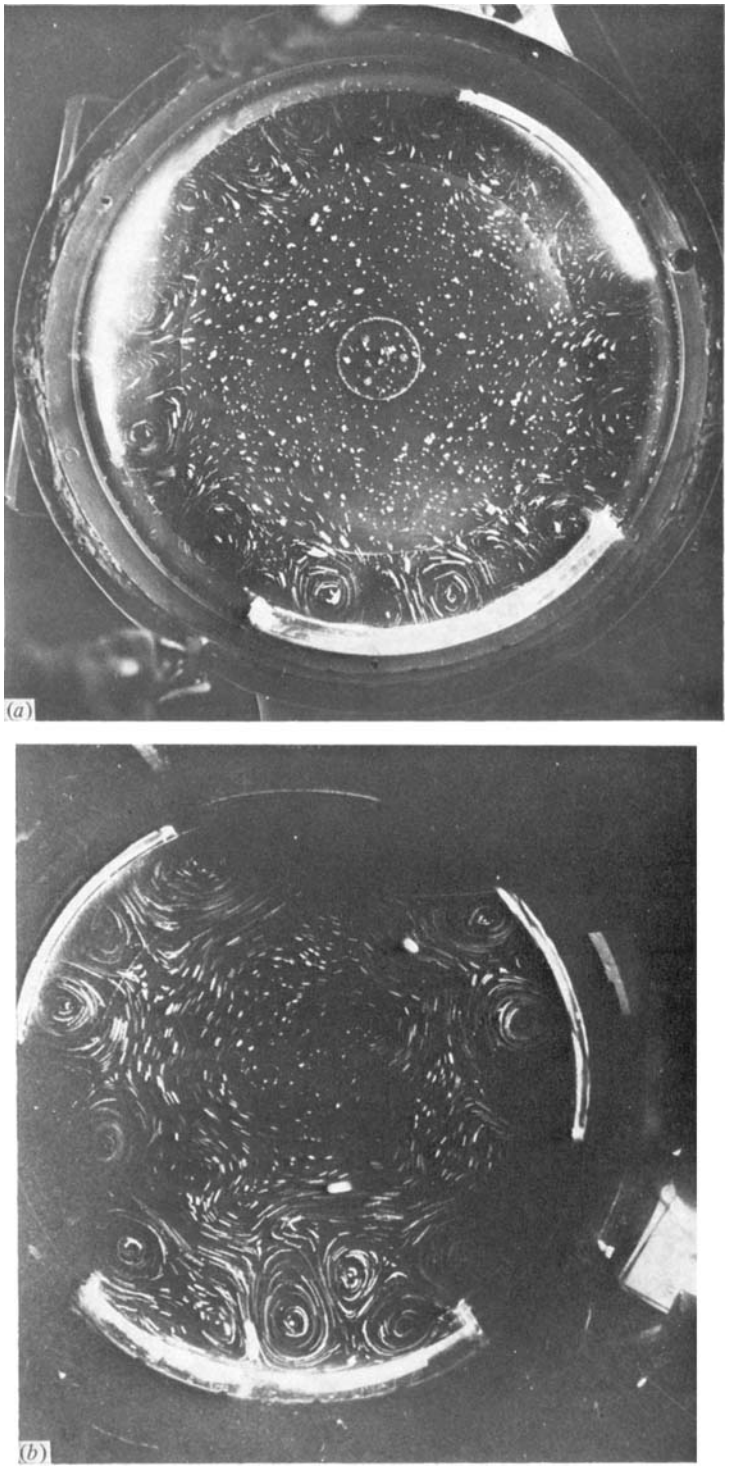

FIGURE 3. (*a*) The Rossby wave transients induced by switching on the westward-travelling ring forcing at the outer boundary. (*b*) The statistically steady state. Laboratory parameter values are: $\Omega = 3{\cdot}06$ rad/s, $\omega = 0{\cdot}4$ rad/s, $H = 7$ cm, $Q = 363$ cm^3/s. Non-dimensional parameters become: $U/fL = 2{\cdot}5 \times 10^{-2}$, $E = 6{\cdot}8 \times 10^{-5}$, $F_r = 0{\cdot}13$ and $U/c = 3{\cdot}3$.

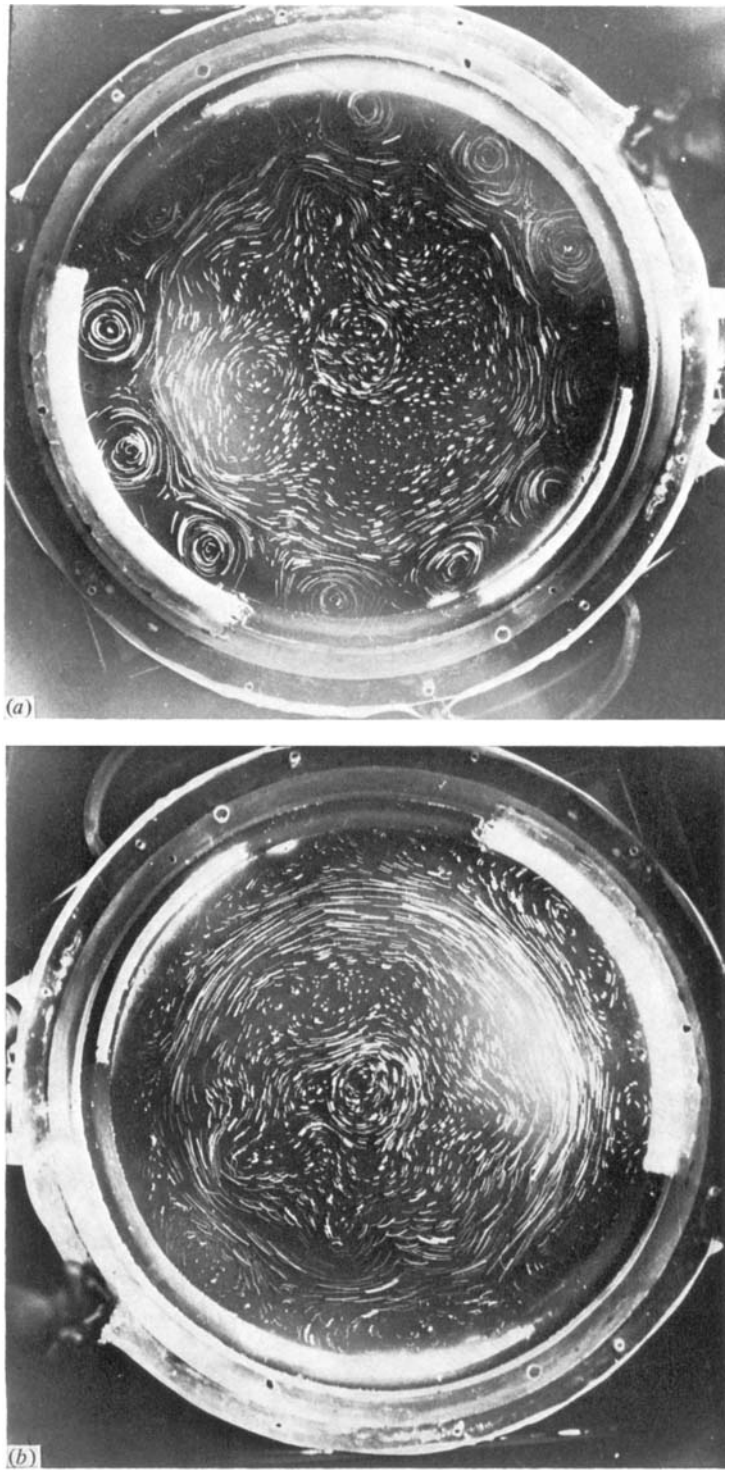

FIGURE 6. (*a*) The statistically steady state. (*b*) The period of decay 20 s after switching off of the driving. Laboratory parameter values are: $\Omega = 3{\cdot}83$ rad/s, $\omega = 0{\cdot}4$ rad/s, $H = 10$ cm, $Q = 363$ cm^3/s.

COLIN DE VERDIÈRE

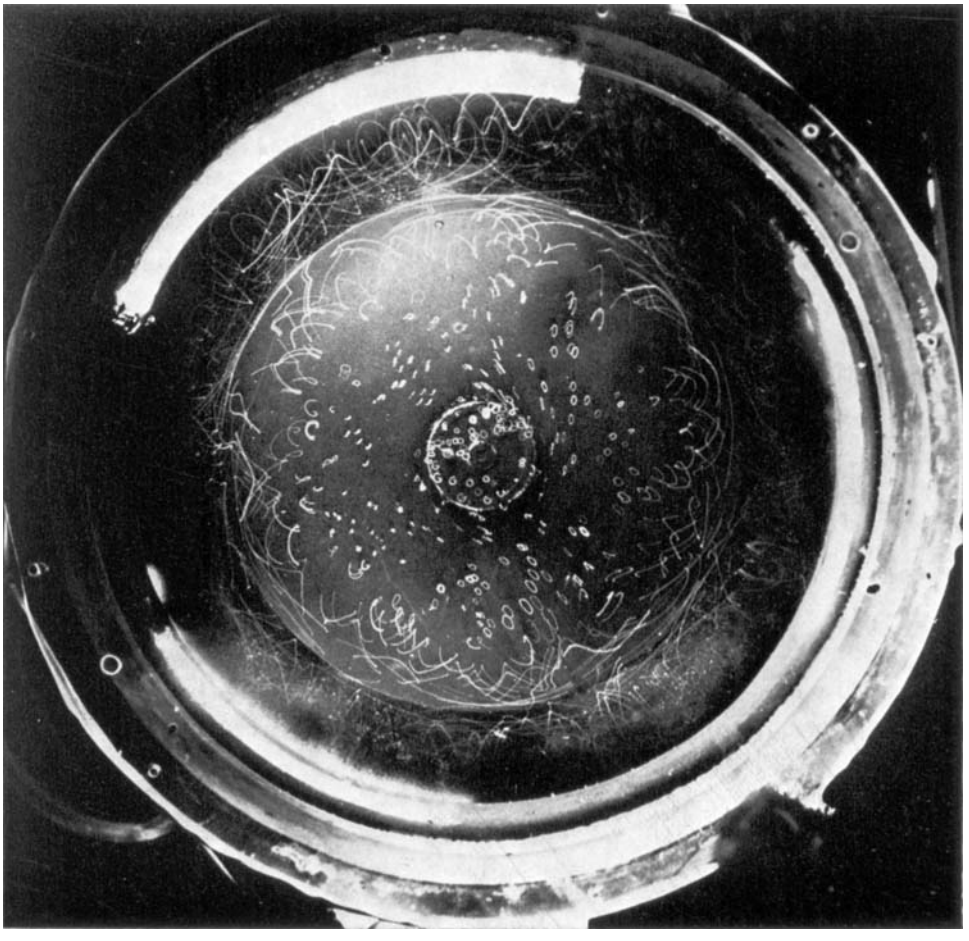

FIGURE 11. A long-exposure photograph revealing the fluid-particle paths in a weak Rossby wave field. The time exposure is equal to the wave period.